ELSEVIER

Biochimica et Biophysica Acta 1231 (1995) 123–138

BBA Biochimica et Biophysica Acta

Review

The dynamics of proton exchange between bulk and surface groups

Menachem Gutman *, Esther Nachliel

Laser Laboratory for Fast Reactions in Biology, Department of Biochemistry, George S. Wise Faculty of Life Sciences, Tel Aviv University, Ramat Aviv 69978, Israel

Received 5 January 1995; revised 25 April 1995; accepted 28 April 1995

Contents

1. Introduction

The role of protons as the carrier of usable energy in bioenergetic processes has been established for a long time [1]. Yet the mechanism of energy transformations, as mediated by protons, has been traditionally investigated by steady-state flux measurements. Steady-state measurements are per definition carried out in a time frame which is much longer than the turnover time of the system. As a result, events faster than the rate-limiting steps had been

* Corresponding author. Fax: +972 3 6415053.

SSDI 0005-2728(95)00074-7

ignored. On the other hand, in the time-resolved domain, the initiation of the reaction is very fast, so that the observer can detect the earliest steps of the reaction. In most enzymic reactions the initiation time cannot be shorter than a few milliseconds, as achieved by rapid mixing systems. Only those reactions which could be initiated by a light pulse, such as photosynthesis or flash dissociation of CO from cytochrome oxidase, were not restricted to the limitation set by rapid mixing.

During the last 10–15 years there has been an increasing number of publications in which the observations of proton transfer reactions breach the millisecond time barrier set by the mixing of fluids. In these studies the system is perturbed by a short light pulse and pH indicators are used to monitor the release or uptake of protons by the enzymic system. Naturally, the favored systems for such experiments are bacterial rhodopsin [2–5] or the photosynthetic system [6–8]. In parallel with these enzymically driven photochemical reactions, another family of observations has appeared. These are studies based on the laser-induced proton pulse [9–15], where specific fluorophores, that shift their pK upon excitation, are used for perturbation of acid-base equilibrium and the physical-chemical properties of the surrounding environment are probed.

The introduction of new observation methodologies, which allow the probing of molecular events in real time (nanosecond to microsecond time scale) necessitates the adoption of new modes of analysis which rely on modern chemical-physical concepts like the Marcus theory for electron [16,17] and proton [18,19] transfer, detailed modeling of electrostatic potentials in microscopic spaces [20,21] or numeric reconstruction of proton transfer reactions in homogeneous [22] or heterogeneous environments [23,24].

At present, when time-resolved instrumentation is becoming prevalent and more investigators have access to such facilities, we wish to present in this review the benefits and pitfalls that can be encountered while studying the dynamic interactions between protons and biomembrane.

2. Protonation of surface group

2.1. The rate constant of protonation

pH indicators are dyes or fluorophores that exhibit a large spectral shift upon binding of a proton. When the protonated moiety of the dye is an oxygen (like the hydroxy or carboxy groups) or a nitrogen (amino), the formation of the covalent bond between the hydrated proton and the electronic orbital of the acceptor atom is much faster than the encounter between the proton and the acceptor atom. As a result, the observer will record the spectral change of the indicator whenever H^+ collides with the indicator. Such a regime, where the chemical reaction is faster than collision between the reactants, is called diffusion-controlled reaction. The rate constant of diffusion-controlled reaction is given by the Debye–Smoluchowski [25] equation, which correlates between well-defined molecular physical parameters and the rate of collision:

$$k_{dc} = \left[4\pi \frac{N}{1000} \cdot \Sigma_D \cdot R_o\right]\left[\frac{\delta}{\exp(\delta) - 1}\right] \times \left[\exp\left(\delta(\kappa R_o/(1 + \kappa R_o))\right)\right] \quad (1)$$

The first term of the equation defines the rate of collision between reactants in the absence of electrostatic interactions. The parameters appearing in the first term are N (Avogadro number), Σ_D (sum of diffusion coefficient of the reactants) and R_o (collision distance). For a free diffusing proton $D_{H^+} = 9.3 \cdot 10^{-5}$ cm^2/s and $R_o \approx 6$ Å, the resulting rate of encounter between H^+ and uncharged target is about $4 \cdot 10^{10}$ M^{-1} s^{-1}.

The other terms in Eq. (1) account for the electrostatic interaction between H^+ and the acceptor. The intensity of the interaction is expressed by the term δ which is the ratio between the Coulomb cage radius R_c and R_o. The former is the distance at which the electrostatic interaction, whether attractive or repulsive, between the reactants equals the thermal energy (e_o is the electronic charge ($4.8 \cdot 10^{-10}$ e.s.u.) and k_B is the Boltzmann constant)

$$R_c = |Z_1 Z_2| e_o^2 / \epsilon k_B T \quad (2)$$

At room temperature and for $|Z_1 Z_2| = 1$, the value of R_c is 7 Å. (The reader should be aware that R_c is also referred to in some texts as the Debye radius or Onsager length.) The nature of the electrostatic interaction is given by the sign of δ, which is equal to that of the charge product ($Z_1 Z_2$). Attractive interactions will have a negative δ value, while repulsive forces are equated with a positive value of δ.

Once a proton (or other charged particle) penetrates the Coulomb cage, its diffusion is biased by the electrostatic interaction. If the interaction is attractive, $\delta < 0$, the ions will collide in less than 1 ns. Repulsive interaction, $\delta > 0$, will cause the particle to be deflected and the probability of encounter will decrease. The relationships between δ and the rate of the reaction is given by the $\delta/(\exp(\delta) - 1)$ term. A strong repulsive potential, $\delta > 1$, shrinks the expression very rapidly. On the other hand, for attractive potential, the expression approaches linearity for $\delta < -3$. Thus, a very positive acceptor can effectively avoid protonation, while realistic negative charges cannot increase the rate of protonation, even by a factor of 10.

The last term in Eq. (1) accounts for the effect of the ionic strength on the rate of reaction between charged particles. It combines δ, the Debye length ($\kappa = 3.3 \cdot 10^{-7} (I)^{1/2}$ (in cm^{-1} units)) and the radius of encounter (R_o) to a an expression which suppresses the intensity of the electrostatic interaction. The larger the charge of the accep-

tor, the more it will be susceptible to screening by ions in solution. Under physiological conditions, in the presence of about 10 mM buffer or substrate, as in many biochemical reaction mixtures, a single charged anion will react with a proton at a rate of about $(2–4)\cdot 10^{10}$ M^{-1} s^{-1}. Rate constants that are smaller than this value suggest some peculiarities of the proton binding site.

2.2. The dissociation of a proton

Proton dissociation, like other biological processes, calls for collaboration between two consenting partners, the acid and the solvent. In this section we shall concentrate on the dynamic aspects of the reaction and its dependence on the nature of the reactants.

The rate of proton dissociation varies over a huge range. A strong acid will surrender its proton to the solvating water within a few picoseconds, while an H_2O molecule will dissociate spontaneously (to H^+ and OH^-) only once within 9 h. Still, these two reactions are basically the same: a transfer of H^+ from the potential well of the donor to that provided by a pre-existing, short lifetime, configuration of water molecules that serve as an acceptor. Consequently, we must distinguish between the properties of the two partners, the acid and the solvent.

The rate of proton transfer; theoretical considerations

Proton transfer between donor and acceptor is generally described, in a schematic way, as a motion along the reaction coordinate from one potential well to another (see Fig. 1). The theory, originally designed to correlate between free energy and rate constants of outer shell electron transfer reactions [16,17] was adapted by Marcus [18,19] for fast adiabatic proton transfer reactions and successfully applied for proton transfer in model systems [26] and for reactions within the active site of carbonic anhydrase [27].

According to the Marcus theory, the proton transfer takes place within a reaction complex (having a finite lifetime) that consists of the donor (DH^+), acceptor (A) and the solvent molecules bound to them. The theory quantitates the rate of the reaction with the energy barrier which the proton has to surmount (ΔG^*).

$$k = Z\exp(-\Delta G^*/k_B T) \tag{3}$$

In this equation, Z is the basic rate of the reaction given that no energy barrier exists

$$Z = R_o^2(8\pi k_B T/\mu)^{1/2} \tag{4}$$

where μ is the reduced mass of the reactants. In most cases, Z is approx. 10^{11} M^{-1} s^{-1}.

The passage of the proton from the donor configuration to the acceptor one is regarded as a fast adiabatic process. It takes place when the potential energy curves of the two states cross each other (see Fig. 1) and the proton enters the potential well of the acceptor state.

The energy required for bringing up the donor configuration to the level where the crossing takes place is the total energy barrier (ΔG^*). Its value is a function of two thermodynamic parameters. One is the intrinsic activation energy (ΔG_o^*) which in some texts is named reorganization energy ($\lambda = 4\Delta G_o^*$). The second is the standard free energy of the reaction (ΔG^o), which in the case of proton transfer is proportional to ΔpK. The three energy terms ΔG^*, ΔG^o and ΔG_o^* are interrelated by Eq. (5).

$$\Delta G^* = \Delta G_o^*(1 + \Delta G^o/4\Delta G_o^*)^2 \tag{5}$$

This function permits quantitation of the contribution of the reactants (ΔG^o) and the solvent (ΔG_o^*) to the overall free energy of activation (ΔG^*). Given that ΔG^o for most proton transfer reactions are known and rates of reaction are measurable, the contribution of the solvent to the rate of the reaction (via ΔG_o^*) can be calculated.

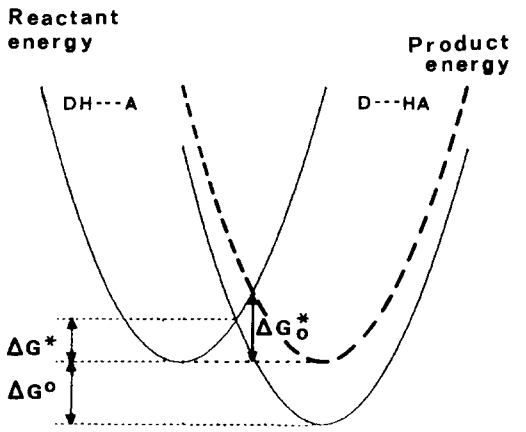

Fig. 1. Schematic presentation of the energy profile associated with proton transfer from a donor complex (left parabola) to the acceptor configuration (right parabola). The ordinate denotes the energy of the systems, while the abscissa is the reaction coordinate. Proton transfer will take place when the energy of the donor system crosses the curve of the acceptor system. ΔG^o is the change in the standard free energy between the two states (proportional to ΔpK). ΔG^* is the activation energy and controls the rate of the reaction (see Eq. 3). ΔG_o^* is the intrinsic activation energy. It is the activation energy of the system in the hypothetical case that $\Delta G^o = 0$ (see the dotted parabola and its crossing point with the donor configuration).

Experimental techniques

The rate of proton transfer is measurable by two main experimental methods: excited-state proton transfer as measured by time-resolved fluorometry and steady-state infrared spectroscopy.

For measuring excited state proton transfer a molecule is pumped to its first electronic singlet state by an ultrashort (picosecond or even femtosecond) laser pulse, which functions as a synchronizing event. The electron distribution in the excited orbital differs from that of the ground state and for certain molecules a large shift of the pK is measured [28]. Aromatic alcohols like naphthols or hydroxypyrene derivatives become more acidic in their excited state ($pK^* \ll pK_o$), while heterocyclic compounds

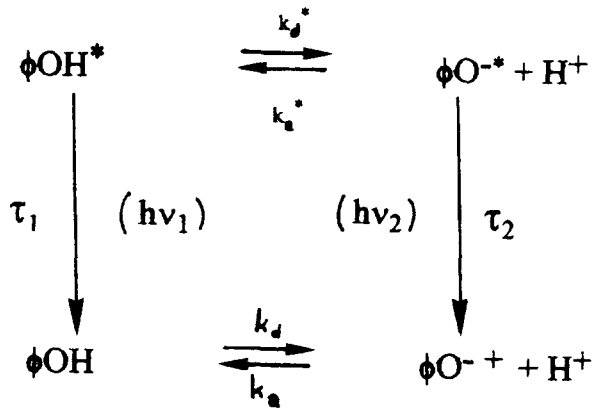

Scheme 1. Schematic presentation of proton dissociation from excited molecules. The ground state acid (ΦOH) is excited to its first electronic singlet state (ΦOH*), which can either decay to ground state with time constant τ_1 while emitting a photon ($h\nu_1$) or dissociate (k_d^*) to a proton and excited anion (ΦO^{*-}). The ΦO^{*-} can recombine with proton (k_a^*) or decay to the ground state with time constant τ_2 and emitting a longer wavelength photon ($h\nu_2$). Please note that all reactants are fully hydrated species.

like acridine or quinoline are more basic ($pK^* \gg pK_0$) (for compilation of pK^* values see Ref. [29]). See Scheme 1.

If the time constant for proton transfer in the *excited state* $(k_d^*)^{-1}$ is comparable with the relaxation of the excited molecules to the ground state (τ_1), then the ΦO^{*-} species can be detected by its own spectral properties. The spontaneous, exoenergetic proton transfer discharges some of the internal energy of the excited molecule and the emission wavelength of the two forms are well distinguished [28]. By measuring the fluorescence intensity at a wavelength characteristic of one form, either ΦOH* or ΦO^{*-}, one can monitor the dynamics of the transition. The high time resolution of current instrumentation [30] provides a detailed mechanistic view of the reaction [22–24].

In contrast with the time-resolving fluorescence spectroscopy, the other method to follow the ultrafast proton transfer between donor-acceptor sites is by steady-state infrared spectroscopy. When a proton can occupy, with comparable probability, two potential wells, its flipping from one site to the other endows the matter with high polarizability [31]. As a result, an alternating electric field synchronized with the intrinsic rate of proton jump between the sites will strongly interact with the matter and its energy will be absorbed. The frequency range in which such absorbance takes place is in the infrared region of the spectrum. When the immediate environment, like solvent molecules, takes part in shaping the potential well, fluctuation in the surroundings of the molecule will change the height of the energy barrier (ΔG^*) and the rate of proton exchange will vary (see Eq. (3)). In the steady-state measurement we sample, simultaneously, all absorbing configurations each with its own absorption frequency. As a result, the multitude of the microscopic states of the population merge into a continuum absorption band in the infrared section of the spectrum [32,33]. The frequency range associated with the IR continuum (1000–3000 cm^{-1}) corresponds to a jump time of a few femtoseconds. Thus, we can regard the proton transfer itself, from a willing donor to a consenting acceptor, as a femtosecond event. The rapid adiabatic transfer is faster than the rearrangement time of the solvent molecules (the lifetime of a hydrogen bond in water is about 2.3 ps, and the rotation time is about 10 ps). Thus we can assume that for a proton transfer to take place, the solvent molecules must already be in the proper configuration to provide the acceptor's potential well.

The effect of pK on the rate of dissociation

The marked difference between the few femtoseconds needed for proton transfer per se versus the time interval between proton dissociation events implies that the rate-limiting step in the dissociation is the formation of the proper situation so that proton will hop from the donor to the solvent. For strong acids in aqueous solution this situation is prevalent, while weak acid molecules very seldom assume a donor position.

For most purposes, the dissociation is taken as a reversible one-step reaction

$$AH_{aq} \underset{k_a}{\overset{k_d}{\rightleftharpoons}} A^-_{aq} + H^+_{aq}$$

and $k_d = k_a \cdot 10^{-pK}$

As k_a for most acids is diffusion-controlled, we find the general approximation $k_d \simeq 2 \cdot 10^{(10-pK)}\ s^{-1}$.

This correlation between the rate of dissociation and the pK of the acid is referred to as the Free Energy Relationship.

This general relationship is valid as long as the observation time is much larger than the dissociation time. When time resolution of the measurements approaches the dissociation time, one-step approximation becomes inadequate and the reactions proceeding within the Coulomb cage must be considered.

2.3. Reactions within the Coulomb cage

The Coulomb cage is the space around an ion in which the electrostatic potential is larger than the thermal energy (see Eq. (2)).

The approach of a proton to the Coulomb cage of an anion is a diffusion-controlled reaction and is measured in the microsecond time-scale. Once the proton gets into the Coulomb cage, its trajectory is dominated by the electrostatic potential and collision with the anion is a matter of a few nanoseconds, a time frame which is comparable with the lifetime of fluorescent pH indicators. Thus evaluation of fluorescent measurements requires the appropriate awareness of the intra-Coulomb-cage dynamics and em-

phasis should be put on the dielectric constant, the diffusion coefficient and the geometry of the reaction space.

Fig. 2 depicts steady-state and time-resolved fluorescence of pyranine inserted in some specific microscopic cavities or when free in water. The steady-state fluorescence exhibits enhanced emission of ΦOH^* when the dye is inside the apomyoglobin's heme binding site and the apparent relaxation of ΦOH^* emission is significantly slower [34]. These features can be explained, in a precise quantitative mode, once we dissect the reaction into elementary, subnanosecond processes taking place within the cage.

The electrostatic potential at a water/membrane (or protein) interface is affected by the dielectric discontinuity at the boundary [35]. As a result, the electrostatic interactions on the surface of the membrane are intensified and can be expressed by a local, position dependent, effective dielectric constant [36]. At the membrane interface, the effective dielectric constant is smaller than that of bulk water [24,34] and the Coulomb cage expands up to few tens of Ångström units. Thus the emergence of a proton from the electrostatic grip of a membrane bound charge will be slower, and the observed dynamics of dissociation will be delayed (see Fig. 2) [24,33,37].

Another term that affects the reactions within the Coulomb cage is the geometry of the reaction space. While considering a proton–anion interaction in bulk water, the reaction space is spherical. But when the dissociating moiety is bound to a membrane [38] or inserted in a defined cavity [37], the dispersion of the proton will not be as in a spheric symmetric environment. Both factors, the local electric field and the non-spherical reaction space, have been treated, quantitatively, by the formalism of Agmon for geminate recombination between a proton and an anion [22,39]. The basic model, described in Fig. 3, consists of an anion (having a radius R_0) surrounded by a homogeneous matrix with a dielectric constant ϵ, and a free proton having a diffusion coefficient of (D_H^+).

The space-time distribution of a proton within the reaction space is calculated by numerical simulation of a proton stepping between equipotential sectors around the central anion. The probability of a proton to step from site i (characterized by electrostatic potential $V_{(i)}$) to site j is given by an equation that combines the diffusion coefficient, geometry and electrostatic potentials [22,39].

$$TP_{i/j} = \left[\frac{D_{H^+}}{\Delta r^2}\right] \cdot \left[f^{(n)}(r_i/r_j)\right] \cdot \left[\exp\left(-R_c(1/r_j - 1/r_i)\right)\right] \quad (6)$$

The equation consists of three terms. The first denotes the frequency of a random proton stepping between two adjacent concentric shells r_i and r_j (see Fig. 3), while the other two quantitate the bias imposed over the random event.

The first term, the stepping frequency, is proportional to the diffusion coefficient. Using the diffusion coefficient of proton in water and a step length equal to a water molecule,

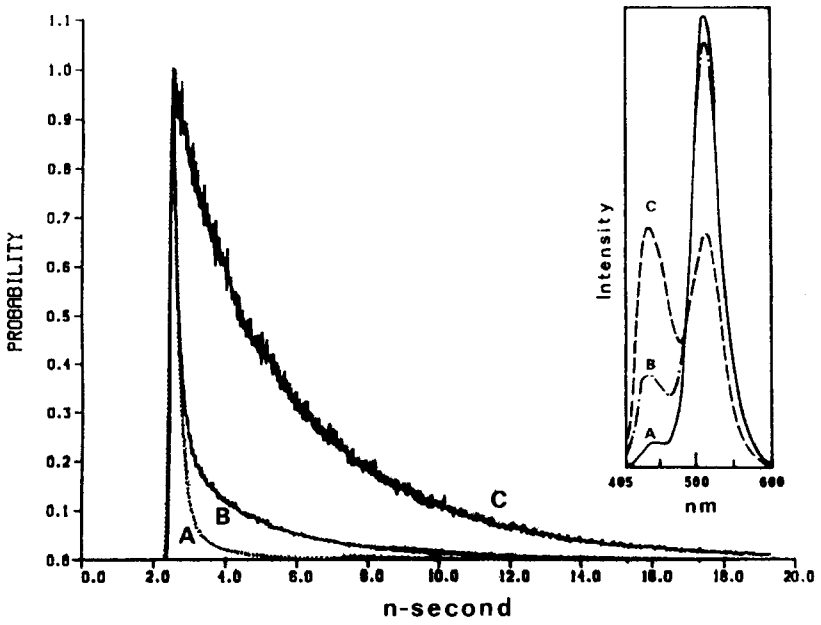

Fig. 2. The effect of the microenvironment on the time resolved and steady state fluorescence of pyranine. The dye was excited in its ΦOH state ($\lambda_{ex} = 400$ nm, pH = 5.5) and the emission was recorded in the time resolved domain ($\lambda_{em} = 430$ nm, main frame) or as steady state fluorescence spectrum (inset). Curve A represents the dynamics measured for the dye when dissolved in pure water. The decay of the ΦOH^* emission is fast and most of the fluorescence emission ($\lambda_{max} = 515$ nm) is of the excited anionic state (ΦO^{*-}) (see inset). Curve B was measured with the dye inserted in the anion specific channel of the Pho.E porin [37] and Curve C is the dye bound to the heme binding site of Apomyoglobin [34]. As seen in the inset, slower relaxation of ΦOH^* is associated with enhanced emission at about 430 nm and reduced emission of the ΦO^{*-} state.

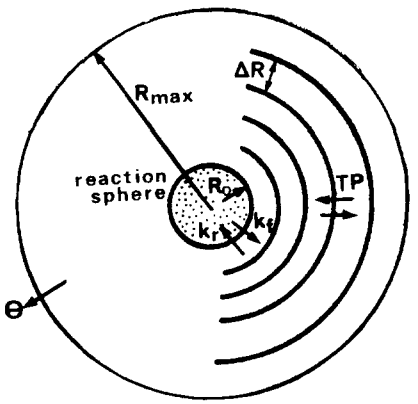

Fig. 3. Schematic description of proton diffusion at the immediate vicinity of an acidic moiety. The proton dissociates from the acid, represented by a sphere with a contract radius R_o at a rate k_f. A proton which is within a contact distance from the anion may be readsorbed with a rate constant of k_r. The diffusion of the proton proceeds by a biased stepping between the equipotential shells that surround the anion. The stepping frequency is a function of the diffusion coefficient, while the bias is made by the entropy of the dilution and the gradient of the electrostatic potential. The expression giving the transition probability (TP) between two adjacent shells (having radii r_i and r_j, respectively) is given in Eq. (5). At R_{max} the proton is either taken up by the bulk or reflected backward ($0 < \alpha < 1$), depending on the definition of the boundary condition. For more details see [34,37,39]).

we obtain a stepping frequency of 10^{11} s^{-1}. This value is comparable to the rotation time of H_2O in water.

The geometric term $f^{(n)}$ (r_i/r_j) is a function which varies with the dimensionality (n) of the space. In a three-dimensional space, like a proton near a protein ($f^{(3)}$ $(r_i/r_j) = r_i/r_j$). In a two-dimensional space, such as the intermembranal space of the mitochondrion, $f^{(2)}$ $(r_i/r_j) = (r_i/r_j)^{1/2}$, while in a one- dimensional environment, as in an ionic channel, $f^{(1)}$ $(r_i/r_j) \equiv 1$.

The last term of Eq. (6) employs the values of R_c and r_i to introduce the effect of the electrostatic gradient on the transition probability. Once the transition probabilities between all adjacent equipotential sectors have been calculated, a numerical procedure can simulate probability densities, ($P_{(r)}$) of proton within the space and the variation of the probability densities with time $P_{(r;t)}$ provides the scenario of the fate of a proton in the reaction space. This model was successfully implemented for reconstruction of proton diffusion in defined microscopic sites having dimensions comparable to the Coulomb cage [22–24,34,37,39,40].

These studies monitored the diffusion of a proton within the apomyoglobin heme binding site [34], the Pho.E channel [37], the interbilayer space of multilamellar liposomes [24] or the inner space of submitochondrial vesicles [40]. The observed dynamics has been reconstructed and the chemical-physical properties which dictate the apparent dissociation dynamics have been determined. These characteristic properties are listed in Table 1.

In all samples listed in Table 1, except for submitochondrial vesicles where information is still missing, the proton emitting dye was adsorbed to the macromolecular structure. In case of proteins, the dye is attracted to positively charged sites (for details see references listed in the table). The binding to phospholipid membrane is also electrostatic in nature. The sulfono moieties of the pyranine are stabilized by interaction with the dipoles of the zwitterionic headgroups.

The measured diffusion coefficient of a proton in these environments was found to be equal to that of bulk water (as on a phospholipid/water interface) or somewhat smaller. This finding negates the prevailing (but not substantiated) assumption that ordering of water at the interface enhances the mobility of protons.

In all sites listed in Table 1, the electrostatic potentials, as characterized by the effective dielectric constant (ϵ_{eff}), are much intensified. In a small cavity like the apomyoglobin heme binding site, the electric potential can be ten times larger than in bulk water. As the dimension of microscopic sites can be smaller than the Debye length of physiological systems, the ionic screening within these cavities will be rather ineffective.

The variation of the activity of water at the interfaces listed in Table 1 will be discussed below.

To provide the reader with an intuitive sense for the dynamics within a microscopic space, we describe in Fig. 4 the spatial-temporal distribution of a proton discharged inside the Pho.E ionic channel. In this three-dimensional presentation the probability of finding a proton (indicated on the ordinate) is given as a function of distance (right side abscissa) and time (left side abscissa). The flux of the proton towards the bulk is given by a motion along right side arrow, while the temporal distribution of proton along the length of the channel is given by the left side arrow. As

Table 1
The physical-chemical properties of microscopic space as gauged by a free diffusing proton

	k_f (s^{-1})	a_{H2O}	ϵ_{eff}	D_{H+} (cm^2/s)	Ref.
H_2O	$7 \cdot 10^9$	1.000	78	$9.3 \cdot 10^{-5}$	[22]
pho.E. (anionic channel)	$5.5 \cdot 10^9$	0.966	24	$(4.0 \pm 0.5) \cdot 10^{-5}$	[37]
Lysosyme (anion binding site)	$2.8 \cdot 10^9$	0.88	13.5	$(4.0 \pm 0.5) \cdot 10^{-5}$	[56]
Apomyoglobin (heme binding site)	$0.22 \cdot 10^9$	0.61	8	$(4.5 \pm 0.5) \cdot 10^{-5}$	[34]
Multilamellar vesicles (PC) (interbilayer space)	$4.0 \cdot 10^9$	0.92	40	$9.3 \cdot 10^{-5}$	[24]
Submitochondrial vesicles (inner space of vesicles)	$2.7 \cdot 10^9$	0.87	20	$2.3 \cdot 10^{-5}$	[40]

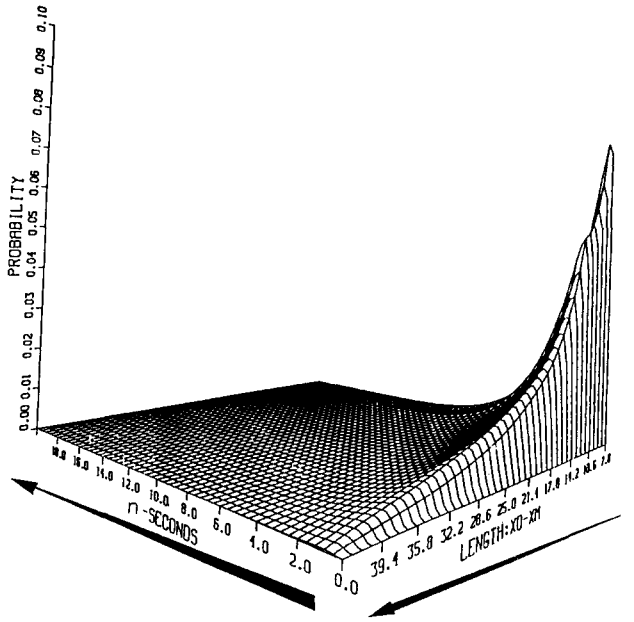

Fig. 4. The spatio-temporal distribution of a proton discharged by an acid ($Z = -1$) within the porin's (Pho.E) channel. The ordinate denotes the probability of finding a proton at distance r_i from the source (right side abscissa) and at time t after the dissociation (left side abscissa). This scenario corresponds with precise reconstruction of the ΦOH^* emission decay fluorescence shown in curve B of Fig. 2.

the reader will note, the channel is emptied of proton in a matter of a few ns.

2.4. The effect of solvent

Biochemical reactions proceed in dilute aqueous solutions. Thus one might conclude that the nature of the solvent is constant in all systems and will have no effect on proton dissociation. That notion is correct for reactions in the bulk but not for interfacial reactions (see above). The interface of a membrane or a protein has a lower *standard* chemical potential for water (μ_{H2O}) [41,42] and the rotational translational motion is slowed down [43,44]. As a result the capacity of water to execute rapid solvation of the proton dissociation product is diminished [45].

The activity of water

Water at an interface is characterized by a reduced standard chemical potential (or vapor pressure) [41,42]. In the present discussion we shall use the term 'activity' (a_{H2O}) which is the ratio between the vapor pressure of a solution (or microenvironment) vs. that of pure water ($\mu = RT \ln(a_{H2O})$). The water molecules most tightly bound to phospholipid membrane have a potential as low as -600 cal/mol ($a_{H2O} = 0.36$) [42]. Similarly, the high density of water (up to 1.5 g/cm^3) calculated for the first hydration shell of a protein in solution [41] implies $a_{H2O} = 0.66$. The effect of water activity on the rate of proton dissociation was studied in concentrated aqueous solutions of strong electrolytes. These salts, when dissolved in water, are strongly hydrated and the activity of water of the solution is reduced. Dynamic measurements revealed that the rate of proton dissociation from excited pyranine decreases with the activity of the water, independently of the electrolyte used for that purpose [43]. The dependence followed an empirical expression:

$$\log k_i = \log k_o - n \log(a_{H2O})_i \quad (7)$$

In this expression k_o and k_i are the rates measured in pure water and in a solution having activity $a(_{H2O})_i$. The number n was found to vary with the nature of the dissociating acid. For compounds like α-naphthol, $n = 4$ [44], while with other compounds values as high as 7–9 were measured [45].

The mechanistic explanation for the dynamic effect is based on the fact that proton transfer per se is faster than the random motion of the solvent molecules. It is the random rotation plus translation of the water molecules that forms a transient configuration which provides a temporary potential well for the dissociating proton. The rate at which proton will fill the well is a function of ΔpK (free energy relationship) and the proximity of the well to the donor as measured along the reaction coordinate. In a microscopic space at the membrane interface, where the water molecules are tightly bound and oriented, the probability of finding the solvating cluster is reduced by a Boltzmannian expression and the number of molecules involved in the reaction.

The dependence of the rate of dissociation on a_{H2O}, once calibrated for a given acidic moiety, can be used for quantitation of a_{H2O}, in microscopic spaces in which the 'gauge' acid can be inserted. That feature had been used by Gutman et al. for measuring a_{H2O} in the heme binding site of apomyoglobin [34], the anionic channel of Pho.E [37], the interbilayer space of multilamellar vesicles [24] or the inner space of submitochondrial vesicles [40]. As shown in Table 1, water molecules which solvate open structures like the interbilayer space of multilamellar liposomes or the big pore of the Pho.E channel have a_{H2O} close to unity. Water in a well-confined space as in the apomyoglobin heme-binding site is tightly bound and may be taken as approximating the conditions in active sites.

Modulation of the solvent at the interface

A special case of interfacial proton dissociation is the presence of other surface groups only a few Ångström units from the dissociating proton. These groups may be instrumental in the primary stabilization of the dissociation product and only later dispatch the proton to the bulk. Measurements with protein or membranal models are presently unavailable, due to the inherent complexity of the surface. Thus the best representation of that effect is where the proximity of an accessory hydroxyl is imposed by inserting proton emitting moieties into well defined microscopic structures. The system suitable for this pur-

pose is the β or γ cyclodextrins. These are cup-shaped polysugar molecules which have a cavity large enough to bind, through hydrophobic interactions, molecules having a diameter of 6–10 Å. The experiments of Chattopadhyah and his co-workers [48–50] and later of Fleming et al. [46] clearly demonstrated that dissociable groups alter their pK as well as rate of dissociation when they are inserted into the 'sugar cup'. In cases where the proton donating moiety (the NH_3^+-group of aminopyrene) was at a proximity to the hydroxy rim of the cup, the dissociation was faster and pK was lowered by about 1 pK unit. This is a case where the local environment acts as a primary proton acceptor which, due to higher basicity [51], accelerates the rate of dissociation.

3. The ensemble properties of membrane

In the previous section we considered the rate of proton interactions with a single site located on a membrane (or protein) surface. In the present one we shall discuss how an assembly of protonable moieties on the surface modulates their dynamics of protonation.

The phosphohead groups on a membrane are space some 7–10 Å apart. On a protein, the side-chains of amino acids can be much closer. At such proximity, the Coulomb cages of the individual groups merge together to form an extended one, smeared over the surface. This expanded site will have a higher probability of binding a proton from the bulk and in parallel, higher reactivity with a base in the bulk. In the present section the various aspects of the interaction of proton with a composite surface will be presented.

3.1. Cluster of proton binding sites

The simplest model that records the mutual interaction between two surface groups, as they exchange a proton with the bulk, consists of two pH indicators, Bromocresol green (BCG) and Neutral red (NR), adsorbed on a neutral micelle [52]. Bromocresol green adsorbed on a neutral micelle has (in its deprotonated state) two negative charges. Neutral red is an uncharged indicator and, when adsorbed to the micelle, is less exposed to the bulk. Thus, the protonation rate of the BCG on the micelle is faster than that of NR [52].

When the two indicators share the same micelle, their protonation dynamics get coupled. As a result the protonation of NR will proceed not only by its direct reaction with bulk protons; it may also abstract a proton from its neighbour. The exchange of protons between the two indicators also affects the dynamics of Bromocresol green. Its rate of deprotonation by bulk acceptor (ΦO^-) is accelerated due to the enhanced reactivity of ΦO^- with the positively charged NRH^+. Thus, we find a situation where the cooperation between the surface groups endows the system with dynamic properties which are a combination of each element of its constituent.

The rate of proton transfer between adjacent groups is fast. Gutman and coworkers measured the exchange of protons among surface groups on mixed micelles [52,53], black lipid membranes [14], purple membranes [54], mitochondrial preparations [40,55] and proteins [15,56]. In all these cases the exchange of protons was noted in the microsecond time scale. Direct NMR measurements of proton exchange among phosphatidylethanolamine headgroups [57] yielded comparable rate constants (10^6 s^{-1}). Thus, we conclude that surface moieties can exchange protons within the microsecond time frame or even faster.

The utilization of a few carboxylates as assistants in the introduction of a bulk proton into an active site is readily exemplified by the reactions at the Q_B site of the reaction center of *R. sphaeroides*, whose three-dimensional structure is known. The reduction of this quinone proceeds by sequential electron transfer steps, followed by uptake of protons. This system is ideal for measuring the coupling between proton and electron transfer. The reducing electrons can be pumped into the quinone system by a short synchronizing light pulse, while the reduction products of the quinone are well characterized by their absorption spectra. Exploitation of these experimental advantages, with support from point mutation, revealed the role of two carboxylates (Asp-L213 and Glu-L212) as initial proton carriers [58] with the assistance of Ser-L223, which transfers the proton to the interior of the protein where the quinone is located [7,59]. It is of importance to point out that, once the proton has been taken up by the surface groups, its further transfer to the quinone radicals is not instantaneous. Actually, it can be the slower step in the overall process [59].

3.2. Evaluation of proton conducting network

While the above example focused our attention to a small site where only a few (2–3) moieties are involved, there are cases where large regions of the protein or the membrane function as proton collecting antenna.

The functioning of the antenna was first demonstrated while measuring the kinetics of protonation of fluorescein molecules, covalently attached to bovine serum albumin (see Fig. 5) [15,60]. Analysis of the results revealed that the major pathway leading to protonation of the dye was initiated by protonation of one of the multitude of carboxylates covering the protein. The initial protonation of the surface was followed by rapid motion of the proton among the carboxylates until it reacted with the dye. This pathway appeared to be very effective. Blocking of as few as about 12% of the carboxylates by amidation [60] sufficed to lower the peak protonation of the dye by about 30%. Blocking of half of the carboxylates almost eliminated the protonation of the dye (see Fig. 5).

The 'proton collecting antennae' have recently been

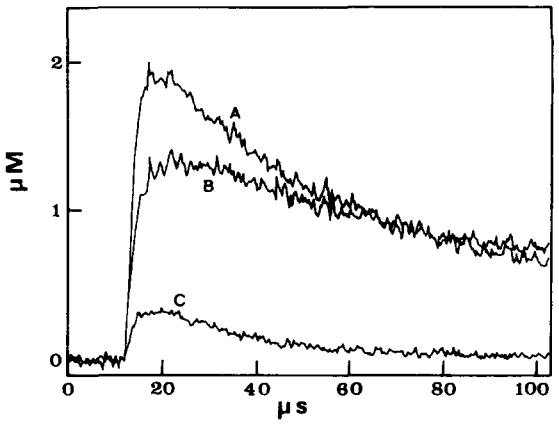

Fig. 5. Pulse protonation dynamics of fluorescein attached to bovine serum albumin. The protein dye adduct (7 fluoresceins per protein, 75 μM with respect to the dye) was dissolved in 1 mM of 2-naphthol-3,6-disulfonate (pH 8.0). The sulfono naphthol was excited by a UV laser pulse and the discharged protons were detected ($\lambda = 496$ nm) by the bleaching of the indicator bound to the protein using the extinction coefficient $\epsilon_{490} = 63 \cdot 10^3\ M^{-1}cm^{-1}$. Curve A was measured with fluorescein-labeled protein. Curves B and C were measured with protein where 12% and 45% of the carboxylates were randomly blocked by amidation. For details see [60].

demonstrated in functional structures like mitochondrial inner membrane [40,55] or purple membrane of *H. halobium* [54]. Both systems were labeled, by fluorescein, on one face of the membrane and suspended in dilute pyranine solution. A short laser pulse excited the pyranine to its first electronic singlet state and the discharged protons upset all acid-base equilibria of the system. The perturbed system was monitored by two measurable parameters: the reprotonation of ΦO^-, which counts the protons missing from the bulk, and protonation of the fluorescein. The difference between the two quantities are protons bound to other surface groups of the membrane (see Fig. 6).

The analysis of the observed signals [54,55] revealed that both the matrix side of the mitochondria and the cytoplasmatic face of the purple membranes exhibited enhanced capacity for trapping protons from the bulk. The other face of the membranes was devoid of this property. The unequal protonation dynamics of the two faces of these membranes is attributed to the higher content of carboxylates as found on the cytoplasmatic face of the purple membrane or the matrix face of the mitochondria.

3.3. The efficiency of proton conducting network

The capacity and efficiency of proton conduction by a network of adjoining Coulomb cages is hard to quantitate by direct experimental approach. On the other hand the model describing the dynamics of a proton in an isolated Coulomb cage (see Section 2.3 above) can be converted into a minimal setup of two cages which transfer a proton between them. The model consists of two identical sites, each characterized by a single R_c value, and the potential of proton located between them is the sum of the attraction to both sites. The simulation of the transfer is initiated by 'discharging' the proton from the source and proceeds until it is absorbed by the sink. The output of this computation is the dynamics of protons accumulated in the sink.

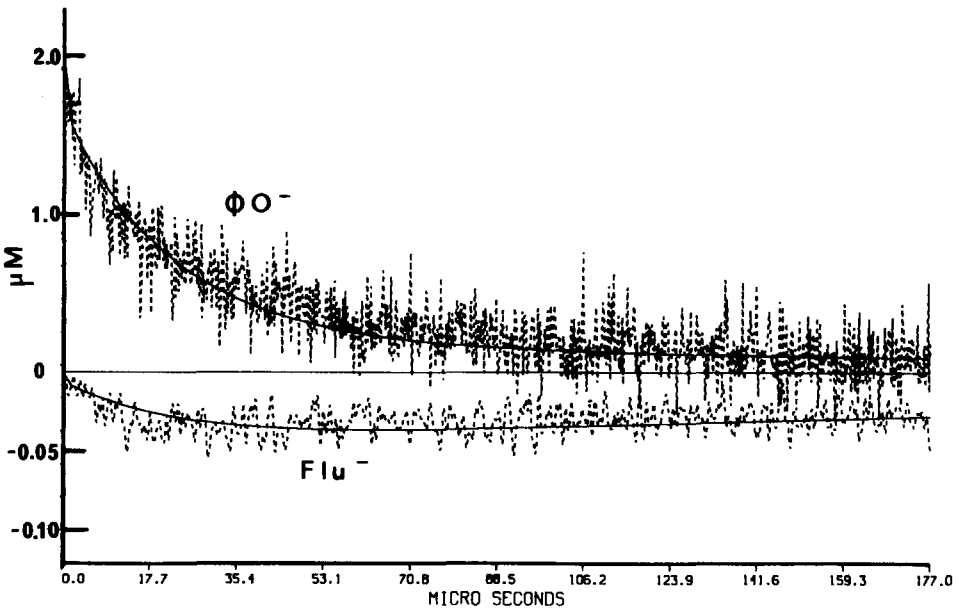

Fig. 6. Dynamic measurement of proton transfer between bulk and *H. Halobium* purple membrane preparation. Purple membranes were labeled by fluorescein (97% efficiency) on lysine 129. The suspension was supplemented by 11.9 μM of pyranine (pH 7.3) and pulsed by UV ($\lambda = 355$ nm) laser pulses. Transient absorbances were measured at the wavelength of ΦO^- ($\lambda = 458$ nm (A)) and of the fluorescein ($\lambda = 496$ nm) absorption bands. Both curves are corrected for the photocycle's proton pumping. Please note that the fluorescein curve (Flu^-), drawn as a negative transient, is drawn on a different scale from that of ΦO^-.

During the passage from source to sink there is a certain probability that the proton will be lost to the bulk. According to Onsager [61], a proton located at a distance r_i from an anion having a Coulomb cage radius of R_c will have a probability P_i to diffuse to the bulk without a single encounter with the anion [61].

$$P_i = \exp(-R_c/r_i) \quad (8)$$

Thus, a proton which managed to propagate from a source up to $r_i = 3R_c$ will have a probability of about e^{-1} to re-encounter with its source. That distance can be taken as the effective boundary of bulk.

Using the parameters that characterize proton diffusion near a phospholipid membrane ($D_{H+} = 9.3 \cdot 10^{-5}$ cm^2/s) and $R_c = 14$ Å for $Z = -1$ ion) we simulated the diffusion of a proton from an isolated source up to $r_i = 42$ Å. These dynamics, shown in Frame A of Fig. 7, imply that within 0.6 ns the population of protons within this space ($r_i < 42$ Å) declines to e^{-1}. This apparent time constant, and the corresponding rate constant $k = \tau^{-1} = 1.7 \cdot 10^8$ s^{-1}, characterizes the dissipation rate to the bulk.

The second frame of Fig. 7B depicts the dynamics of passage from source to sink, under conditions where the proton dissipates to the bulk. The curves correspond to the accumulation of protons in the sink, where the distances between the two sites are 12, 24, 36 and 60 Å. At 12 Å apart, about 99.5% of protons leap from source to sink without wandering to the bulk. As the distance increases, so does the loss to the bulk and the yield of protein reaching the sink dwindles.

The efficiency of the mechanism should be reexamined upon expansion of the minimal two sites model into a large number of sites packed on a membrane and evaluate the effectiveness of the mechanism under physiological conditions. An array of negative charges, located few Ångströms apart on a surface, will be effectively screened by counterions even at low ionic strength. Any site within the array which is temporarily occupied by a counterion breaks the continuity of the system and the conductive path will be fragmented into short sections which are equal or shorter than κ^{-1}. Thus the efficiency of the mechanism is expected to hinge not only on the proximity between the elements but also on the ionic strength. At physiological conditions it will operate over very short stretches.

3.4. Macroscopic measurements of proton diffusion at interface

While the above section explicitly limited the surface enhanced dispersion of protons to very short time and length intervals, there have been reports, based on experimental observations, indicating abnormally fast propagation of protons at water/lipid monolayer interfaces [62–69].

In these experiments a monolayer of lipids is formed on the water/air interface and physical methods are used for monitoring how protonic current, or excess of acidity, propagates at the interface. The most critical factor in the analysis of these experiments is the level of confidence that whatever is measured is indeed a sole representation of the monolayer/water interface. When the width of the hydration layer is only 1–3 nm, the problems of eliminating the bulk signal is quite appreciable. In the following section we shall examine these observations:

Conductivity measurements

In these experiments the conductivity of an aqueous phase is measured while a monolayer of phospholipids, or fatty acids, is spread over its surface [62–65]. The distinc-

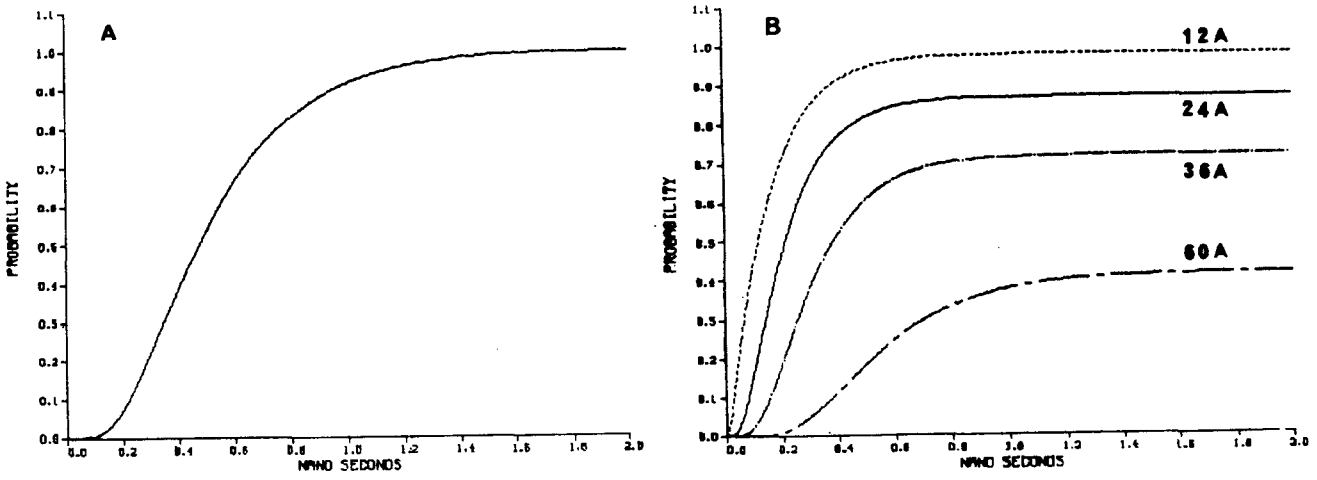

Fig. 7. Theoretical calculation of proton transfer between source and sink with losses to the bulk. The model consists of source and sink, each having $R_c = 14$ Å, where a proton is released in one and trapped by the other. Frame A depicts the accumulated probability of finding in the bulk a proton released from isolated (no sink) source. The apparent time constant of the dispersion corresponds to a rate constant of $1.7 \cdot 10^9$ s^{-1}. Frame B depicts the dynamics of accumulation of proton in a sink placed at a varying distance (as marked in the figure) from the source. The dwindling yield of protons in the sink is due to their loss to the bulk.

tion between the conductivity of the bulk and that of the monolayer/water interface is achieved by two methods. One group [63,64] measured the direct current while gradually compressing the monolayer. The second group [65] was looking for a rapid change in electric conductivity as the spreading monolayer came into contact with the electrodes. In both cases the incremental conductance attributed to the monolayer conductivity is rather small (less than 10% with respect to bulk conductance).

The observation is explained by assuming that when the hydrophilic headgroups are brought into close contact, they exchange protons among them, which appears as an additional conductive pathway. As the monolayer is compressed to the point of collapse, and its pressure increases steeply with reduction of surface, the extra conductivity is rapidly lost.

These measurements are very difficult to execute and their reproducibility was investigated by Menger and coworkers [62]. Menger improved the method by replacing the atmosphere above the cell by nitrogen (to remove CO_2), utilized an automatic dipping device to ensure reproducible positioning of the electrodes, looked for an optimal DC voltage and even inserted another set of electrodes, not in contact with the monolayer, to serve as an internal control. In spite of all these precautions, it was found that the baseline readings were unstable and some of the instabilities indeed reproduced the observation that compression of the monolayer increased the conductance. Yet, if the measuring current was switched from DC [63–65] to alternating current [62] in order to prevent polarization artifacts, the nature of the results was inverse and decreased conductance was noted when a monolayer was formed. The decrease in conductivity associated with formation of continuous monolayer may reflect the lower conductivity of the hydration layer with respect to the water/air interface [62].

Spreading of acid under monolayer

The experiments of Tocanne, Teissie and their associates [66–69] were advocated as a straightforward approach. A Langmuir trough is filled with aqueous solution of buffer (1–200 mM) and covered by a monolayer of lipid. At one side of the monolayer, up to 1.5 ml (depending on the buffer concentration) of 3 M HCl is injected into a well-stirred (90 rpm) compartment and spreading of acidity is monitored on a macroscopic scale. To prevent the spreading of acid through the bulk two barriers separate between the point of injection and the mass of water that supports the surface under study (see Fig. 8). The spreading of the acid is monitored at a fixed distance from the point of injection (4–4.5 cm) by continuous measurement of the emission of a fluorescent indicator attached covalently to a phospholipid molecule. The time needed for the initiation of the acidification, ΔT_{H+}, and extent of fluorescence decrement, ΔF, are measured (see inset to figure). These time measurements are carried out under

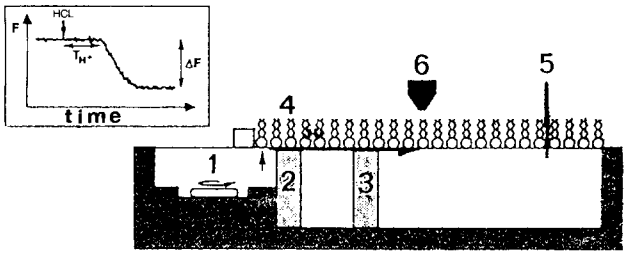

Fig. 8. The instrumental setup for measuring the dispersion of acid at the water-monolayer interface: 1, injection cell stirred at 90 rpm; 2 and 3, barriers that prevent the spreading of acid into the main bulk compartment; 4, the monolayer that projects into the acid injection cell, and bound at 5 by a moving barrier that also records the monolayer pressure. The fluorescence changes of a pH indicator, covalently bound to the lipid, is measured at point 6. Inset, an example of a typical recording redrawn after Gabriel and Teissie [68]).

varying compression pressure that modulate the surface area per lipid molecule at the monolayer.

The interpretation of the results has been based on a hypothetical model characterized by three, non identical, diffusion coefficients. One is for lateral diffusion at the interface, the second is for lateral diffusion in the bulk and the third one is for transfer of proton from interface to bulk. The diffusing species is considered to be a proton while the contribution of the buffer as a carrier of acidity has been ignored. The model propagates the 'proton' in a small two-dimensional grid made of six layers, each containing 30 space elements. The 'diffusion coefficient' of proton along each layer, and passage between layers, was varied in order to obtain a scenario where the dispersion in the upper layer was faster than in the lower ones. The results of these computations were compared qualitatively with the experimental observations of the acidification of the water/air interface.

This analysis produces a ratio between the diffusion coefficients of proton in the interface and subphase. According to the authors the diffusion coefficient at the molecular layer of the water/lipid interface was estimated to be 20-times larger than in the bulk, but no absolute units were given. The claim of the authors was that the excessive rate of diffusion is derived from rapid exchange of protons between the phosphohead groups. The efficiency of that process is said to be abolished when the lipids are compressed to the gel state.

The criticism of these conclusions will be centered on three main issues: (1) Does the spreading of acid on the surface proceed by diffusion? (2) What is the force field that retains the excess acid on the surface? (3) To what extent do the calculated parameters represent molecular properties?

(1) Acceptance of a diffusion model in macroscopic experiments should be made cautiously, due to the inherent slowness of the process. Thus, at first, we have to ascertain that no other translational mechanisms are operative. For this reason we shall concentrate on the *control* experi-

ments of Toccane, Teissie and their colleagues, where they state that the accelerated proton spreading on surface is not operating.

The excess acidity added to the injection compartment propagates in a diffused front shaped like the integral of a Gaussian function. The acidification of the indicator, at the point of observation, will appear when the front edge of the propagating acid will lower the local pH to the level of the indicator's pK. If we assume that the front edge of the acidic wave (1% of the added acid) is sufficient to overcome the buffer capacity of the subphase then, using the Gaussian probability function, we find this edge to be at a distance of 2.3σ from the point of injection (where σ is the standard deviation of the Gaussian). The dependence of σ on time is given by $\sigma = (2Dt)^{1/2}$. Based on these assumptions, we find that σ should be about 17–18 mm for the first 1% of the acidification front to reach a distance of 4–4.2 cm. The time required for that is about 260 min. This time estimation is significantly larger than 45 min which Teissie and co-workers report for their control experiments [68]. This discrepancy suggests that the spreading of acidity is supported by some convection current.

At that point it might be added that the acid dispersion experiments were done with a continuous stirring (90 rpm) of the acid injection compartment. The stirring rate accelerated the spreading of acid from the injection cell. At 120 rpm turbulence on the surface of the monolayer was observed [66]. Yet the effect of stirring was measured even at 20 rpm. To account for the requirement of constant stirring it was stated that the stirring could carry the protons from the bulk to the interface over some energy barrier. This barrier "is abolished by strong stirring which provides protons with kinetic energy and (the barrier) reappears as soon as the stirring is suppressed" [66]. As kinetic energy of a molecule in condensed phase is determined *exclusively* by temperature through the Boltzmann distribution, we cannot avoid the conclusion that small eddies energized by the stirring bar participate in the transport of acid to the main compartment.

(2) The persistence of protons at the interface. The design of the diffusion trough is such that acid, going over the first barrier, will be diluted in the space before the second one (see Fig. 8). The observation was that the excess acidity continues to expand and adheres to the surface. The persistence of proton at the interface is observed in the presence of 100 mM NaCl, or even 0.2 M phosphate buffers [67] where the electrostatic attraction of a proton to the surface is practically nil (50% of the surface charge is neutralized by Na^+ at 10 Å from the surface [39]). This implies that some other mechanism, like thermal flotation, originating from the heat of dilution of the 3 M HCl (1 kcal/mol) retains the excess acidity at the top layer, while convection currents spread it along the trough.

(3) Macroscopic measurements do not yield molecular properties. When excess acid is spread over a surface carrying protonable sites with a buffered subphase, the parameter characterizing the observed signal is not the diffusion coefficient of a proton which is a molecular parameter, but an effective parameter that is a combination of many terms (see Eq. (9), below). Thus, whatever the apparent diffusion coefficient obtained by Tocanne, Teissie and their colleagues is, it must be broken down to its components before any molecular mechanism can be derived.

4. Proton transfer in buffered solution

Except for the intrathylakoid space, which topologically is extracellular, all other cellular cavities are filled with well buffered solutions. The buffer capacity is made of phosphates, phosphorylated compounds (sugars or nucleotides like ATP, ADP), carboxylic groups of substrates or fixed buffering groups on proteins and membrane's surfaces.

While buffered species do not affect each other's titration curves, they are adverse competitors in the kinetic mode. Thus after pulse acidification of a solution, the protonation of one site will be affected by the presence of buffers, and in more than one mode. On the one hand, the buffer will compete for free protons, thus slowing the rate of direct protonation. On the other hand, free diffusing buffer may act as a proton carrier delivering a proton to a hard to get site. The capacity of HN_3 to deliver a proton to the Schiff base of mutated bacterial rhodopsin is an excellent example. The normal path for the Schiff base reprotonation is through Asp-96, which is located on the cytoplasmatic channel of the protein. Replacement of aspartate by asparagin (D96N) deletes the proton donating moiety with subsequent delay in the relaxation of the M state of the photocycle [70,71]. The proton in this mutant must diffuse the whole length of the cytoplasmatic section of the channel in order to reprotonate the Schiff base. Addition of N_3^- acting as a hydrophobic proton carrier (HN_3) largely facilitates the passage of proton, with subsequent acceleration of the M → N transition.

In the present section of the review we shall discuss the various aspects in which the buffer affects the dynamics of bulk surface proton transfer.

4.1. Diffusion of proton in buffered solutions

Diffusion of protons in aqueous solutions is through the exchange of hydrogen bonds-covalent bonds between solvated protons and the surrounding water matrix (a Grotthuss mechanism). Because of that mechanism the diffusivity of protonic charge in water ($D_{H+} = 9.3 \cdot 10^{-5}$ cm^2 s^{-1}) is larger than that of any other ion. It is even faster than the self diffusion of H_2O in water ($D_{H2O} = 2.5 \cdot 10^{-5}$ cm^2 s^{-1}). The dispersion of excess acid in solution, be it

on a macroscopic scale or as a part of the energy conservation machinery, is not a diffusion of proton. It is a summation of many processes like diffusion of free proton, uptake and release of protons by buffers, diffusion of protonated buffer molecules, exchange of protons between mobile and sessile (membrane bound) buffer moieties and proton exchange between adjoining sessile buffers. Due to the multiplicity of modes for dispersion of acid in solution the analysis of experimental observation does not yield the diffusion of H^+.

The correlation between the various terms that contribute to the apparent dispersion of acidity and the molecular events associated with the process had been analyzed by Junge and McLaughlin [72]. In their treatment the overall process is taken as a sum of fluxes by all acid carriers (H^+, OH^- and buffers), where each buffer (B_i) is characterized by its dissociation constant (K_i) and diffusion coefficient (D_i). The contribution of all carriers to the measured value is proportional to their buffer capacity (β_i) normalized by the total one (β_{tot})

$$D_{eff} = D_{H^+}\left(\frac{2.3[H^+]}{\beta_{tot}}\right) + D_{OH^-}\left(\frac{2.3[OH^-]}{\beta_{tot}}\right) + \frac{\sum_i D_i \beta_i}{\beta_{tot}} \quad (9)$$

where the buffer capacity of the species B_i is:

$$\beta_i = 2.3[H^+] \cdot \left(1 + ([B_i]K_i)/([H^+] + K_i)^2\right)$$

The last term in Eq. (9) sums up the individual contribution of all buffering species present in the system. Mobile buffers, having a diffusion coefficient of small solutes ($r < 25$ Å) $D_M = 1 \cdot 10^{-6}$–$1 \cdot 10^{-5}$ cm^2/s, will increase the overall diffusivity in proportion to their buffering capacity (β_i/β_{tot}). Sessile buffers ($D_S < 5 \cdot 10^{-7}$ cm^2/s) will have a negligible contribution as a proton carrier. On the other hand, due to their intrinsic buffering capacity, sessile buffers increase β_{tot}, which appears as a denominator in all the terms of Eq. (9). As a result, the presence of a sessile buffer suppresses the apparent diffusivity, irrespective of what other carriers are present in the system. The effects of added buffers on the diffusivity of acid are demonstrated by the following example: In a dilute solution ($\beta_M = 1$ mM, pH 6) of mobile buffer having a diffusion coefficient 10-times smaller than a free proton ($D_M = 0.1\ D_H^+$) the dispersion of added acid will have an apparent value of $D_{eff} = 0.101\ D_{H+}$. Replacement of the buffer by a sessile on having a diffusion coefficient of $D_S = 3 \cdot 10^{-3}\ D_{H+}$ will reduce the dispersion of acid in the unstirred layer to $D_{eff} = 3 \cdot 10^{-3}\ D_{H+}$. If both buffers are present, then the dispersion of acid in the unstirred layer will be $D_{eff} = 0.05\ D_{H+}$. Thus, we can generally state that buffering will always reduce the diffusivity of acid below the value measured in pure water. What is more, any diffusion coefficient measured by dispersion of acidity in a buffered solution is only an apparent one which does not represent the molecular parameter of D_{H+}.

The capacity of sessile buffer moieties to retard the dispersion of acid in the unstirred layer, as first demonstrated by Junge and Polle [73], can account for the measurements of Dencher and his colleagues [74]. In their experiments, purple membrane sheets 0.6 μm in diameter labeled by fluorescein on their cytoplasmatic side were excited by a short light pulse. The protons driven by the photocycle were released on the extracellular face and the time delay required for their detection by the indicator on the other face of the membrane was measured. The apparent diffusion coefficient, as calculated from their measurements ($9 \cdot 10^{-7}$ cm^2 s^{-1}) is very close to the value predicated by Eq. (9) ($3.4 \cdot 10^{-7}$ cm^2 s^{-1}). The coherence between the experimental value and the theoretical prediction implies that, at the surface of the membrane, there are no other processes which are not explicitly expressed by Eq. (9).

4.2. Collisional proton transfer

Under physiological conditions protonation of proteins (or membranes) proceeds almost exclusively through buffer molecules present in the reaction space. The pseudo-first-order rate constant of protonation by free protons ($k_H[H^+]$) is smaller than that of collisional proton transfer ($k_c[BH]$) due to the large excess of BH over H^+ as found in a buffered solution (BH > 10^{-3} M) close to neutrality ($H^+ < 10^{-6}$ M).

Unlike the reaction of free protons (or hydroxyls) which interact in a diffusion-controlled reaction, buffer-mediated proton transfer is not essentially so. The collision between a proton donor DH and acceptor A is generally diffusion-controlled, but the ensuing reactions can be much slower [75], depending on the ΔpK between the reactants and on the reorganization energy (ΔG_0^*) of the immediate environment (see Section 2.2). In such cases an intermediate complex (DH · · A) is formed. The existence of the intermediate is inferred from an overall rate constant, which is slower than a rate of a diffusion controlled reaction.

These dynamics can be analyzed as a sequential two-step reaction and the rate of the intracomplex proton transfer reaction can be determined.

The capacity of that treatment to reveal the effect of water on the rate of proton transfer was demonstrated by Raviv [26], who studied the transfer of protons within a reaction complex [DH · · A] made of acridinum (donor) and an indicator, fluorescein or Bromothymol blue, serving as an acceptor. The rate constants of the intracomplex proton transfer were calculated and their values were analyzed according to Eqs. (3), (4) and (5). The reorganization energies, as measured in pure water, were comparable to the values reported by Cohen and Marcus [18]. When the reactions were measured in concentrated solu-

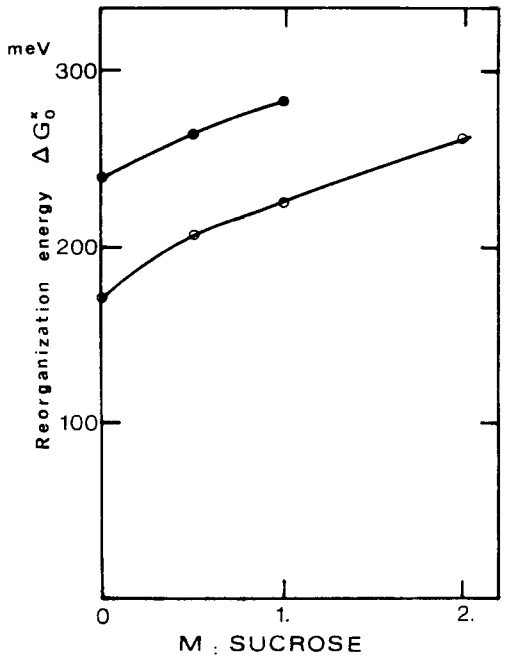

Fig. 9. The dependence of the reorganization energy, measured for proton transfer, from acridinium to indicator, on the concentration of sucrose in the reaction mixture. The kinetics were measured in the time-resolved domain using photogenerated acridinium ions as proton donor and either fluorescein (●) or Bromothymol blue (○) as acceptors. The kinetics were analyzed to determine the rate of intracomplex proton transfer and the reorganization energy was calculated according to Eqs. (3)–(5). For details see [26].

tions of sucrose (0.5–2 M), there was a continuous, smooth increase of the reorganization energy (see Fig. 9). At that range of solute concentrations, the average distance between the sucrose molecules is comparable to the dimension of the reaction complex. Thus, the immediate environment, where proton transfer takes place, is gradually replaced from neat water to water solvating the sucrose. Apparently, the energy required to deform the donor configuration to that of the acceptor state increases when the water molecules solvate the sucrose. Considering the fact that the surface of membranes or protein is covered by their own solvation shell, where water molecules have a lower mobility [43,44], it becomes apparent that the state of solvation of these structures will modulate the rate of proton transfer on their surface. The same reaction will proceed at different loci at varying rates.

4.3. Proton mobility on semi-dried surfaces

The biomembrane is a heterogeneous macroscopic structure covered by multitudes of sites which interact with the solvent, protons and among themselves. The proton reactivity of each site is determined exclusively by the physical properties of the immediate environment, yet due to the close proximity between sites, one may affect the reactivity of the other. The interaction between sites, or the connectivity on the surface, is provided by the water. The capacity of water to amalgamate the surface can be measured by the dependence of the dielectric dispersion (α dispersion) [76–78] or electric conductivity [79] of semi-dried samples (proteins or biological samples as germinating seeds) on their water content. In these experiments the sample is placed as a dielectric insulator in a capacitor, and the dependence of the capacitance is measured at varying humidities.

It was found that, at the above critical level of hydration, the capacitance increases very steeply due to long range proton polarizability which we can consider as a macroscopic equivalence of the molecular mechanism leading to the continuum IR absorption.

The sharp appearance of protonic polarizability is explained within the terms of the percolation theory of Careri [78]. According to this model, proton can move on the surface by many alternating routes which are made of overlapping Coulomb cages connected by the hydration layer of the membrane. As water molecules are removed, the continuity of the network is lost and at a certain critical value, the long range connectivity, is totally lost. The dependence of the long range protonic conductivity on the state of hydration was measured directly [79] or inferred from dielectric dispersion for a variety of samples [78]. In all measurements the dependence was in accord with the theoretical predictions. What is more, enzymic or physiological activities were expressed only at the point where the connectivity was well established.

These observations exploited the proton mobility as a gauge particle for probing the level of hydration of the surface and their conclusions simply state that biological machinery attains its optimal conditions when suitably wetted.

In the well-hydrated state, the surface is exposed to bulk water which, for thermodynamic and kinetic reasons, is a strong attractor for protons. Thus under physiological conditions bulk water serves as the bridging matrix and the mobile buffer is the main proton carrier.

4.4. The boundaries of 'local' enhanced reactions

Biochemical literature employs the expression 'local' (proton) and 'non-local' (proton) as self explanatory terms. As discussed in this review, these terms can be precisely defined. When a proton is discharged from a protogenic site there is a brief period when its concentration (or probability density) close to the site is higher than the average concentration. This transient state can be evaluated by time and length parameters.

For a given concentration of protons in solution we can define a space element (having a radius R_{eq}) which is permanently occupied by the bulk proton ($R_{eq} = 11.8 \times \sqrt[3]{[H^+]}$, given in Å units). A proton emerging from a protogenic site will diffuse away from the site and its radial distance (r_i) will increase up to R_{eq}. From that time

on, the probability of finding a proton at R_{eq} from the site will be time-independent and equal to the average value. Within that short period when $r_i < R_{eq}$, any reactant located within the r_i from the source will have a higher than average probability to bind the proton. This period of grace is self-limiting. In unbuffered solution at pH 6, R_{eq} is about 1200 Å and the local enhancement of reaction within this space will fade within the 0.7 μs needed for the proton to diffuse up to R_{eq}.

The time and space boundaries of local enhanced reactivity shrink dramatically when buffer is added to the solution. In the presence of buffer, the local enhancement will be limited to the space element determined by homogenously distributed buffer molecules. At a moderate concentration of buffer (10 mM) the locally enhanced region will be limited to about 50 Å from the site and will last not more than 1 ns.

The packing of proteins on biomembranes and the folding of membranes that push one enzyme towards the other affect the border between 'local' and bulk by the same mechanism. Proteins carry a multitude of proton-binding sites, and only a few of them are within the active site. The tight packing of proteins, near a protogenic enzyme, actually pushes the border of bulk towards the protogenic site as the buffer moieties on the surface compete with the active site for the proton.

To sum up, bulk and local are defined by time and space boundaries, and usage of these terms must be done with the relevance to the length of observation period and spatial distribution of the reaction space. Otherwise their intuitive interpretation may be misleading.

Acknowledgements

This research is supported by grants from the United States–Israel Binational Science Foundation (91-00226) and the Office of Naval Research (N00014-94-0533).

References

[1] Mitchell, P. (1966) Chemiosmotic coupling in oxidative and photosynthetic phosphorylation, Glynn Research Laboratories, Bodmin.
[2] Lozier, R.H., Bogomolini, R.A. and Stoeckenius, W. (1975) Biophys. J. 15, 955–963.
[3] Mathies, R.A., Lin, S.W., Ames, J.B. and Pollard, W.T. (1991) Annu. Rev. Biophys. Biophys. Chem. 20, 491–518.
[4] Souvignier, G. amd Gerwert, K. (1992) Biophys. J. 63, 1393–1405.
[5] Lanyi, J.K. (1993) Biochim. Biophys. Acta 1183, 241–261.
[6] Maroti, P. and Wraight, C.A. (1988) Biochim. Biophys. Acta 934, 329–347.
[7] McPherson, P.H., Okamura, M.Y. and Feher, G. (1993) Biochim. Biophys. Acta 1144, 309–324.
[8] Lavergne, J. and Junge, W. (1993) Photosynth. Res. 38, 279–296.
[9] Gutman, M. (1984) Methods Biochem. Anal. 30, 1–103.
[10] Gutman, M. (1986) Methods Enzymol. 127, 522–538.
[11] Gutman, M., Nachliel, E., Gershon, E., Giniger, R. and Pines, E. (1983) J. Am. Chem. Soc. 105, 2210–2216.
[12] Nachliel, E. and Gutman, M. (1984) Eur. J. Biochem. 143, 83–88.
[13] Nachliel, E., Ophir, Z. and Gutman, M. (1987) J. Am. Chem. Soc. 109, 1342–1345.
[14] Gutman, M., Nachliel, E., Bamberg, E. and Christensen, B. (1987) Biochim. Biophys. Acta 905, 390–398.
[15] Yam, R., Nachliel, E. and Gutman, M. (1988) J. Am. Chem. Soc. 110, 2636–2640.
[16] Marcus, R.A. (1968) J. Phys. Chem. 72, 891–899.
[17] Jortner, J. (1980) Biochim. Biophys. Acta 594, 193–230.
[18] Cohen, A.O. and Marcus, R.A. (1968) J. Phys. Chem. 72, 4249–4256.
[19] Marcus, R.A. (1982) Faraday Discuss. Chem. Soc. 74, 7–15.
[20] Sancho, M. and Martinez, G. (1991) Biophys. J. 60, 81–88.
[21] Klapper, I., Hagstrom, R., Fine, R., Sharp, K. and Honig, B. (1986) Proteins: Struct. Funct. Genet. 1, 47–59.
[22] Pines, E., Huppert, D. and Agmon, N. (1988) J. Chem. Phys. 88, 5620–5630.
[23] Gutman, M., Nachliel, E. and Kiryati, S. (1992) Biophys. J. 63, 274–280.
[24] Gutman, M., Nachliel, E. and Kiryati, S. (1992) Biophys. J. 63, 281–290.
[25] Eigen, M., Kruse, W., Maas, G. and De Maeyer, L. (1964) Prog. React. Kinet. 2, 287–303.
[26] Raviv, S. (1991) M.Sc. thesis, Tel Aviv University.
[27] Silverman, D.N., Tu, C., Chen, X., Tanhauser, S.M., Kresge, A.J. and Laipis, P.J. (1993) Biochemistry 32, 10757–10762.
[28] Weller, A. (1961) Prog. React. Kinetics 1, 189–214.
[29] Ireland, J.F. and Wyatt, P.A.H. (1976) Adv. Phys. Org. Chem. 12, 131–221.
[30] Fleming, G.R. (1986) Chemical Applications of Ultrafast Spectroscopy, Oxford University Press, Oxford.
[31] Zundel, G. (1983) in Biophysics (Hoppe, W., Lohmann, W., Markl, H. and Zigler, H., eds.), pp. 243–255, Springer, Berlin.
[32] Leberle, K., Kampf, I. and Zundel, G. (1989) Biophys. J. 55, 637–648.
[33] Zundel, G. (1992) Trends Phys. Chem. 3, 129–156.
[34] Shimoni, E., Tsfadia, Y., Nachliel, E. and Gutman, M. (1993) Biophys. J. 64, 472–479.
[35] Mathias, R.T., Baldo, G.J., Manivannan, K. and McLaughlin, S. (1992) In Electrified Interfaces in Physics, Chemistry and Biology (Guidelli, R., ed.), p. 473, Kluwer, London.
[36] Gilson, M.K., Rashin, A., Fine R. and Honig, B. (1985) J. Mol. Biol. 183, 503–516.
[37] Gutman, M., Tsfadia, Y., Masad, A. and Nachliel, E. (1992) Biochim. Biophys. Acta 1109, 141–148.
[38] Kraayenhof, R., Sterk, G.J. and Wong Fong Sang, H.W. (1993) Biochemistry 32, 10057–10066.
[39] Huppert, D., Pines, E. and Agmon, N. (1990) J. Opt. Soc. Am. B7, 1545–1550.
[40] Kotlyar, A.B., Borovok, N., Kiryati, S., Nachliel, E. and Gutman, M. (1994) Biochemistry 33, 873–879.
[41] Alary, F., Durup, J. and Sanejouand, Y.-H. (1993) J. Phys. Chem. 97, 13864–13876.
[42] Parsegian, V.A., Fuller, N. and Rand, R.P. (1979) Proc. Natl. Acad. Sci. USA 76, 2750–2754.
[43] Steinhaff, H-J., Kramm, B., Hess, G., Owerdieck, C. and Redhart, A. (1993) Biophys. J. 65, 1486–1495.
[44] Raghavan, K., Reddy, M.R. and Berkowitz, M.L. (1992) Langmuir 8, 233–240.
[45] Huppert, D., Kolodney, E., Gutman, M. and Nachliel, E. (1982) J. Am. Chem. Soc. 104, 6949–6953.
[46] Hansen, J.E., Pines, E. and Fleming, G.R. (1992) J. Phys. Chem. 96, 6904–6910.
[48] Chattopadhyay, N., Dutta, R. and Chowdhury, M. (1989) J. Photochem. Photobiol. 47, 249–257.
[49] Chattopadhyay, N., Chakraborty, T., Nag, A. and Chowdhury, M.J. (1990) Photochem. Photobiol. 50, 199–204.

[50] Chattopadhyay, N. (1991) J. Photochem. Photobiol. 52, 31–36.
[51] Pines, E. and Fleming, G.R. (1991) J. Phys. Chem. 95, 10448–10457.
[52] Gutman, M. and Nachliel, E. (1985) Biochemistry 24, 2941–2946.
[53] Nachliel, E. and Gutman, M. (1988) J. Am. Chem. Soc. 110, 2629–2635.
[54] Nachliel, E., Gutman, M. and Dencher, N., unpublished results.
[55] Gutman, M., Kotlyar, A.B., Borovok, N. and Nachliel, E. (1993) Biochemistry 32, 2942–2946.
[56] Yam, R., Nachliel, E., Kiryati, S., Gutman, M. and Huppert, D. (1991) Biophys. J. 59, 4–11.
[57] Ralph, E.K., Lange, Y. and Redfield, A.G. (1985) Biophys. J. 48, 1053–1057.
[58] Takahashi, E. and Wraight, C.A. (1992) Biochemistry 31, 855–866.
[59] Leibl, W., Sinning, I., Ewald, G., Michel, H. and Berton, J. (1993) Biochemistry 32, 1958–1964.
[60] Yam, R. (1988) in Ion Pumps: Structure, Function and Regulation (Stein, W.D., ed.), pp. 279–282, Alan R. Liss, New York.
[61] Onsager, L.J. (1934) J. Chem. Phys. 2, 599–603.
[62] Manger, F.M., Richardson, S.D. and Bromley, G.R. (1989) J. Am. Chem. Soc. 111, 6893–6894.
[63] Morgan, H., Taylor, D.M. and Oliveira, O.N. (1991) Biochim. Biophys. Acta 1062, 149–156.
[64] Morgan, H., Taylor, D.M. and Oliveira, O.N. (1988) Chem. Phys. Lett. 150, 311–314.
[65] Sakurai, I. and Kawamura, Y. (1989) Biochim. Biophys. Acta 985, 347–350.
[66] Prats, M., Tocanne, J.F. and Teissie, J. (1985) Eur. J. Biochem. 149, 663–668.
[67] Gabriel, B., Prats, M. and Teissie, J. (1994) Biochim. Biophys. Acta 1186, 172–176.
[68] Gabriel, B. and Teissie, J. (1991) J. Am. Chem. Soc. 113, 8818–8821.
[69] Tocanne, J.F. and Teissie, J. (1990) Biochim. Biophys. Acta 1013, 111–142.
[70] Tittor, J., Soell, C., Osterhelt, D., Butt, H.J. and Bamberg, E. (1989) EMBO J. 8, 3477–3482.
[71] Cao, Y., Varo, G., Chang, M., Ni, B., Needleman, R. and Lanyi, J.R. (1991) Biochemistry 30, 10972–10979.
[72] Junge, W. and McLaughlin, S. (1987) Biochim. Biophys. Acta 890, 1–5.
[73] Junge, W. and Polle, A. (1986) Biochim. Biophys. Acta 848, 256–273.
[74] Heberle, J., Riesle, J., Thiedemann, G., Osterhelt, D. and Dencher, N.A. (1994) Nature 370, 379–382.
[75] Shoup, D.L. and Szabo, A. (1982) Biophys. J. 40, 33–39.
[76] Bruni, F. and Leopold, C. (1991) Physiol. Plant 81, 359–366.
[77] Hawkes, J.J. and Pethig, R. (1988) Biochim. Biophys. Acta 952, 27–36.
[78] Rupley, J.A., Gratton, E. and Careri, G. (1983) Trends Biochem. Sci. 8, 18–22.
[79] Bone, S. (1991) Biochim. Biophys. Acta 1078, 336–338.